Available online at www.sciencedirect.com

ScienceDirect

Procedia IUTAM 11 (2014) 44 – 57

Procedia IUTAM

www.elsevier.com/locate/procedia

Nonlinear Interfacial Wave Phenomena from the Micro- to the Macro-Scale

Forced and unforced flexural-gravity solitary waves

Philippe Guyenne[a], Emilian I. Părău[b,*]

[a]*Department of Mathematical Sciences, University of Delaware, DE 19716, USA*
[b]*School of Mathematics, University of East Anglia, Norwich, NR4 7TJ, UK, Tel: +441603592965*

Abstract

Flexural-gravity waves beneath an ice sheet are investigated. Forced waves generated by a moving load as well as freely propagating solitary waves are considered for the nonlinear problem as proposed by Plotnikov and Toland[21]. In the unforced case, a Hamiltonian reformulation of the governing equations is presented in three dimensions. A weakly nonlinear analysis is performed to derive a cubic nonlinear Schrödinger equation near the minimum phase velocity in two dimensions. Both steady and time-dependent fully nonlinear computations are presented in the two-dimensional case, and the influence of finite depth is also discussed.

Selection and peer-review under responsibility of scientific committee of Nonlinear Interfacial Wave Phenomena from the Micro- to the Macro-Scale

Keywords: finite depth, flexural-gravity waves, forced waves, Hamiltonian theory, solitary waves

1. Introduction

In recent years, there has been a renewed interest in hydroelasticity problems dealing with the interaction between moving fluids and deformable bodies. Such problems not only entail considerable mathematical challenges but also have many engineering applications[16]. An important area of application is that devoted to hydroelastic (or flexural-gravity) waves in polar regions where water is frozen in winter and the resulting ice cover is transformed e.g. into roads and aircraft runways, and where air-cushioned vehicles are used to break the ice. A major difficulty in this problem has to do with modelling the ice deformations subject to water wave motions. Theories based on potential flow and on the assumption that the ice cover may be viewed as a thin elastic sheet have been widely used[24]. In this context, most studies have considered linear approximations of the problem, which are valid only for small-amplitude water waves and ice deflections.

Intense waves-in-ice events, however, have also been reported and their analysis indicates that linear theories are not adequate for describing large-amplitude ice deflections (e.g.[18]). In the last few decades, a number of numerical and theoretical investigations have used nonlinear models based on Kirchhoff–Love plate theory to analyse two-dimensional hydroelastic waves in ice sheets. For example, Forbes[9,10] computed periodic finite-amplitude waves using a Fourier series expansion technique. Părău and Dias[22] derived a forced nonlinear Schrödinger equation for the envelope of ice-sheet deflections due to a moving load, and showed that solitary waves of elevation and depression

*Corresponding author
E-mail address: e.parau@uea.ac.uk (Emilian I. Părău).

2210-9838
Selection and peer-review under responsibility of scientific committee of Nonlinear Interfacial Wave Phenomena from the Micro- to the Macro-Scale
doi:10.1016/j.piutam.2014.01.047

exist for certain ranges of water depth. Bonnefoy et al.[2] examined numerically the same nonlinear problem of moving load on ice, through a high-order spectral approach, and found a good agreement with theoretical predictions of Părău and Dias[22]. Hegarty and Squire[15] simulated the interaction of large-amplitude water waves with a compliant floating raft such as a sea-ice floe, by expanding the solution as a series and evaluating it with a boundary integral method. Vanden-Broeck and Părău[26] computed periodic waves and generalised solitary waves on deep-water using a series truncation method. Milewski et al.[19] considered hydroelastic waves on deep water, in both forced and unforced regimes, with the forced regime being equivalent to a moving load. For the unforced problem, they derived a nonlinear Schrödinger equation which indicates that small-amplitude solitary wavepackets do not exist in the deep-water case. They also performed direct time-dependent computations, based on conformal mapping, which reveal stable large-amplitude solitary waves of depression coexisting with background radiation. Părău and Vanden-Broeck[23] addressed the three-dimensional problem in deep water and computed solitary lumps due to a steadily moving pressure. However, although they adopted fully nonlinear equations for the fluid, the ice sheet was modelled by the linear Euler–Bernoulli plate. In a similar context, Xia and Shen[28] established a 5th-order Korteweg–de Vries (KdV) equation for two-dimensional hydroelastic waves on shallow water, and Haragus-Courcelle and Ilichev[14] derived a three-dimensional generalisation of the 5th-order KdV equation.

Recently, Plotnikov and Toland[21] used the special Cosserat theory of hyperelastic shells, satisfying irrotational flow and Kirchhoff's hypothesis, to derive nonlinear equations governing the interaction between a thin elastic sheet and an ideal ocean beneath it. Unlike the Kirchhoff–Love model, this formulation explicitly conserves elastic potential energy. In the present paper, we take advantage of this conservative property in the unforced case to write an explicit Hamiltonian form of the hydroelastic problem in Eulerian coordinates, extending the Hamiltonian formulation of the water wave problem by Zakharov[30] and Craig and Sulem[8]. This new Hamiltonian formulation of the hydroelastic problem is given in the general three-dimensional case and for arbitrary depth. To accomplish this, the Dirichlet–Neumann operator is introduced to reduce the original Laplace problem to a lower-dimensional system involving quantities evaluated at the fluid-ice interface only. Following this procedure, Guyenne and Părău[12] investigated two-dimensional hydroelastic solitary waves on deep water, through both weakly nonlinear analysis and direct numerical simulations, and extension of their work to finite depth is provided in[13]. They calculated both depression and elevation waves, and addressed stability issues. We review some of their results in the present paper and present a new type of time-dependent solutions. More recently, Milewski and Wang[20] proposed a Benney–Roskes–Davey–Stewartson system for three-dimensional weakly nonlinear hydroelastic waves on finite depth, based on the formulation of Plotnikov and Toland[21].

We first examine the linearised case. Similarly to gravity-capillary water waves, an important property of the hydroelastic problem is that its linear dispersion relation exhibits a minimum $c_{\min}$ at which the phase and group velocities coincide. In the unforced case, for small- but finite-amplitude two-dimensional waves with speeds c near $c_{\min}$, we derive a nonlinear Schrödinger (NLS) equation using the Hamiltonian modulational approach of Craig et al.[5,6]. Based on the sign of its coefficients, we find that this NLS equation is of focusing type below a critical depth, similar to results of Părău and Dias[22], but its soliton solutions are unstable. Larger-amplitude two-dimensional waves for $c < c_{\min}$ are computed by solving the full steady equations with a boundary-integral method. Interestingly, their profiles can be well approximated by NLS solutions in finite depth, despite being outside the regime of validity of the NLS equation. A large family of depression solitary waves are found, including overturning waves for c much lower than $c_{\min}$ and sufficiently large depth. For very shallow water, depression waves cannot reach a sufficiently high amplitude to overturn as they are bounded by the fluid depth.

The stability of these solitary waves is also investigated by performing direct numerical simulations in time with a high-order spectral method[8,11,29]. Thanks to its analyticity properties, the Dirichlet–Neumann operator has a convergent Taylor series expansion in which each term can be determined recursively. This series expansion combined with the fast Fourier transform leads to an efficient and accurate numerical scheme for solving the full Hamiltonian equations. For $c < c_{\min}$, the instability of small-amplitude solitary waves is confirmed by our time-dependent computations. However, larger-amplitude solitary waves of depression are found to be stable. In addition to freely propagating waves, forced solutions by a moving load are also computed.

The remainder of the paper is organised as follows. Section 2 presents the mathematical formulation of the hydroelastic problem in three dimensions. The Dirichlet–Neumann operator is introduced and the Hamiltonian equations of motion are established. From this Hamiltonian formulation, a weakly nonlinear model for two-dimensional hydroe-

lastic waves is derived and analysed in § 3. Numerical results are shown and discussed in § 4. Finally, concluding remarks are given in § 5.

2. Mathematical formulation

2.1. Equations of motion

We consider a three-dimensional fluid of uniform finite depth h beneath a continuous thin ice sheet. The fluid is assumed to be incompressible and inviscid, and the flow to be irrotational. The ice sheet is modelled using the special Cosserat theory of hyperelastic shells in Cartesian coordinates (x, y, z) [21], with the (x, y)-plane being the bottom of the ice sheet at rest and the z-axis directed vertically upwards. The vertical deformation of the ice is denoted by $z = \eta(x, y, t)$. The fluid velocity potential $\Phi(x, y, z, t)$ satisfies the Laplace equation

$$\nabla^2\Phi = 0, \qquad \text{for } (x, y) \in \mathbb{R} \times \mathbb{R}, \quad -h < z < \eta(x, y, t). \tag{1}$$

The nonlinear boundary conditions at $z = \eta(x, y, t)$ are the kinematic condition

$$\eta_t + \Phi_x\eta_x + \Phi_y\eta_y = \Phi_z, \tag{2}$$

and the dynamic condition

$$\Phi_t + \frac{1}{2}|\nabla\Phi|^2 + g\eta + P + \frac{\mathcal{D}}{\rho}\mathcal{F} = 0, \tag{3}$$

where

$$\mathcal{F} = 2\left\{\frac{1}{\sqrt{a}}\left[\partial_x\left(\frac{1+\eta_y^2}{\sqrt{a}}\partial_x\mathcal{H}\right) - \partial_x\left(\frac{\eta_x\eta_y}{\sqrt{a}}\partial_y\mathcal{H}\right) - \partial_y\left(\frac{\eta_x\eta_y}{\sqrt{a}}\partial_x\mathcal{H}\right) + \partial_y\left(\frac{1+\eta_x^2}{\sqrt{a}}\partial_y\mathcal{H}\right)\right] + 2\mathcal{H}^3 - 2\mathcal{K}\mathcal{H}\right\},$$

with

$$a = 1 + \eta_x^2 + \eta_y^2, \qquad \mathcal{K} = \frac{1}{a^2}(\eta_{xx}\eta_{yy} - \eta_{xy}^2), \qquad \mathcal{H} = \frac{1}{2a^{3/2}}\left[(1+\eta_y^2)\eta_{xx} - 2\eta_{xy}\eta_x\eta_y + (1+\eta_x^2)\eta_{yy}\right].$$

Hereinafter, subscripts are shorthand notation for partial/variational derivatives (e.g. $\Phi_t = \partial_t\Phi$). In two dimensions, the dynamic condition reduces to

$$\Phi_t + \frac{1}{2}|\nabla\Phi|^2 + g\eta + P + \frac{\mathcal{D}}{\rho}\left(\kappa_{ss} + \frac{1}{2}\kappa^3\right) = 0, \tag{4}$$

where κ is the curvature of the fluid-ice interface and s is the arclength along this interface. In terms of $\eta(x, t)$, the curvature is given by

$$\kappa = \frac{\eta_{xx}}{(1+\eta_x^2)^{3/2}},$$

and therefore

$$\kappa_{ss} + \frac{1}{2}\kappa^3 = \frac{1}{\sqrt{1+\eta_x^2}}\partial_x\left[\frac{1}{\sqrt{1+\eta_x^2}}\partial_x\left(\frac{\eta_{xx}}{(1+\eta_x^2)^{3/2}}\right)\right] + \frac{1}{2}\left(\frac{\eta_{xx}}{(1+\eta_x^2)^{3/2}}\right)^3.$$

The system is completed with the condition at the bottom,

$$\Phi_z = 0 \qquad \text{at } z = -h. \tag{5}$$

In the infinite-depth limit ($h \to \infty$), Eq. (5) is replaced by

$$|\nabla\Phi| \to 0 \qquad \text{as } z \to -\infty.$$

The constant $\mathcal{D}$ is the coefficient of flexural rigidity for the ice sheet, ρ the density of the fluid, g the acceleration due to gravity, and P the external pressure distribution exerted on the ice sheet. By definition, if $P > 0$, the pressure acts downwards. The dynamic condition (3) is obtained from the Bernoulli equation[21]. The inertia of the thin elastic plate is neglected, so the plate acceleration term is not considered here (see[24] for an explanation). We also assume that the elastic plate is not pre-stressed and neglect plate stretching.

The dispersion relation for the linearised problem with solutions of the form $e^{\mathrm{i}(lx+my-\omega t)}$ is

$$c^2 = \left(\frac{g}{k} + \frac{\mathcal{D}k^3}{\rho}\right)\tanh(hk), \tag{6}$$

where $k = \sqrt{l^2+m^2}$ and $c = \omega/k$ is the phase speed. The same dispersion relation (6) is obtained if we consider uniform plane waves with the wavenumber k in the x-direction. It can be shown that the phase speed $c(k)$ has a minimum $c_{\min}$ at $k = k_{\min}$ for any parameter values see e.g.[24,22]. At this minimum, the phase velocity and group velocity are equal.

Another critical speed in finite depth is the long-wave limit $c_0 = \sqrt{gh}$ as $k \to 0$. In this long-wave regime, a 5th-order KdV equation can be derived[13,14,28]. We will here concentrate on the modulational regime, for wave speeds near $c_{\min}$.

If $P = 0$, the total energy

$$H = \frac{1}{2}\iint_{-\infty}^{\infty}\int_{-h}^{\eta}|\nabla\Phi|^2 dzdydx + \frac{1}{2}\iint_{-\infty}^{\infty}\left[g\eta^2 + 4\frac{\mathcal{D}}{\rho}\mathcal{H}^2\sqrt{a}\right]dydx, \tag{7}$$

together with the impulse (or momentum)

$$I = \iint_{-\infty}^{\infty}\int_{-h}^{\eta}\nabla_x\Phi\, dzdydx,$$

where $\nabla_x = (\partial_x, \partial_y)^\top$, and the volume (or mass)

$$V = \iint_{-\infty}^{\infty}\eta\, dydx, \tag{8}$$

are invariants of motion for (1)–(5). The first integral in (7) represents kinetic energy, while the second integral represents potential energy due to gravity and elasticity.

2.2. Hamiltonian formulation

In the case $P = 0$, and following[30,8], we can reduce the dimensionality of the Laplace problem (1)–(5) by introducing $\xi(x,y,t) = \Phi(x,y,\eta(x,y,t),t)$, the trace of the velocity potential on $z = \eta(x,y,t)$, together with the Dirichlet–Neumann operator (DNO)

$$G(\eta)\xi = (-\nabla_x\eta, 1)^\top \cdot \nabla\Phi\big|_{z=\eta}, \tag{9}$$

which is the singular integral operator that takes Dirichlet data ξ on $z = \eta(x,y,t)$, solves the Laplace equation (1) for Φ subject to (5), and returns the corresponding Neumann data (i.e. the normal fluid velocity there).

In terms of these boundary variables, Eqs. (1)–(5) can be rewritten as

$$\eta_t = G(\eta)\xi, \tag{10}$$

$$\xi_t = -\frac{1}{2(1+|\nabla_x\eta|^2)}\Big[|\nabla_x\xi|^2 - (G(\eta)\xi)^2 - 2(G(\eta)\xi)\nabla_x\xi\cdot\nabla_x\eta + |\nabla_x\xi|^2|\nabla_x\eta|^2 - (\nabla_x\xi\cdot\nabla_x\eta)^2\Big] - g\eta - \frac{\mathcal{D}}{\rho}\mathcal{F}, \tag{11}$$

which are Hamiltonian equations for the canonically conjugate variables η and ξ, extending Zakharov's formulation of the water wave problem to hydroelastic waves. Equations (10) and (11) have the canonical form

$$\begin{pmatrix}\eta_t\\ \xi_t\end{pmatrix}=\begin{pmatrix}0&1\\-1&0\end{pmatrix}\begin{pmatrix}H_\eta\\ H_\xi\end{pmatrix}, \tag{12}$$

whose Hamiltonian

$$H=\frac{1}{2}\int\!\!\int_{-\infty}^{\infty}\left[\xi G(\eta)\xi+g\eta^2+4\frac{\mathcal{D}}{\rho}\mathcal{H}^2\sqrt{a}\right]dydx, \tag{13}$$

corresponds to the total energy (7).

2.3. Dirichlet–Neumann operator

In light of its analyticity properties[7], the DNO can be expressed as a convergent Taylor series expansion

$$G(\eta)=\sum_{j=0}^{\infty}G_j(\eta), \tag{14}$$

where each term G_j can be determined recursively[8,29]. More specifically, for $j=2r>0$,

$$\begin{aligned}G_{2r}(\eta)=&\frac{1}{(2r)!}G_0(|D_x|^2)^{r-1}D_x\cdot\eta^{2r}D_x\\&-\sum_{s=0}^{r-1}\frac{1}{(2(r-s))!}(|D_x|^2)^{r-s}\eta^{2(r-s)}G_{2s}(\eta)\\&-\sum_{s=0}^{r-1}\frac{1}{(2(r-s)-1)!}G_0(|D_x|^2)^{r-s-1}\eta^{2(r-s)-1}G_{2s+1}(\eta),\end{aligned} \tag{15}$$

and, for $j=2r-1>0$,

$$\begin{aligned}G_{2r-1}(\eta)=&\frac{1}{(2r-1)!}(|D_x|^2)^{r-1}D_x\cdot\eta^{2r-1}D_x\\&-\sum_{s=0}^{r-1}\frac{1}{(2(r-s)-1)!}G_0(|D_x|^2)^{r-s-1}\eta^{2(r-s)-1}G_{2s}(\eta)\\&-\sum_{s=0}^{r-2}\frac{1}{(2(r-s-1))!}(|D_x|^2)^{r-s-1}\eta^{2(r-s-1)}G_{2s+1}(\eta),\end{aligned} \tag{16}$$

where $D_x=-\mathrm{i}\nabla_x$ and $G_0=|D_x|\tanh(h|D_x|)$ are Fourier multiplier operators. In the infinite-depth limit ($h\to\infty$), G_0 reduces to $|D_x|$[12].

Although the mathematical formulation of the hydroelastic problem is presented here in the general three-dimensional case, we will restrict our weakly nonlinear analysis and direct numerical simulations to two dimensions in the next sections, following Guyenne and Părău[12,13].

3. Weakly nonlinear wave model

In this section, we analyse the weakly nonlinear regime for small-amplitude waves in the modulational regime. We apply the Hamiltonian perturbation approach[3,5,6], which is especially suitable for the present Hamiltonian formulation of the hydroelastic problem. An advantage of this approach is that it naturally associates a Hamiltonian to the equations of motion at each order of approximation. Changing variables through canonical transformations and expanding the Hamiltonian (13) are the main ingredients. Below we only give a brief description of the derivation of the weakly nonlinear model in the present context and refer the reader to[3,5,6] for further details.

3.1. Canonical transformations

The first step is a normal mode decomposition defined by

$$\eta = \frac{1}{\sqrt{2}} a^{-1}(D_x)(v+\overline{v}) + \widetilde{\eta}, \qquad \widetilde{\eta} = \mathbb{P}_0\eta, \tag{17}$$
$$\xi = \frac{1}{\sqrt{2}\mathrm{i}} a(D_x)(v-\overline{v}) + \widetilde{\xi}, \qquad \widetilde{\xi} = \mathbb{P}_0\xi,$$

where

$$a(D_x) = \sqrt[4]{\frac{g + \mathcal{D}D_x^4/\rho}{G_0}},$$

and $(\widetilde{\eta}, \widetilde{\xi})$ are the zeroth modes representing the mean flow. The overbar represents complex conjugation, and $\mathbb{P}_0$ is the projection that associates to (η, ξ) their zeroth-frequency components. Note that now $D_x = -\mathrm{i}\partial_x$ in the two-dimensional case. As a result, the canonical system (12) is transformed to

$$\begin{pmatrix} v_t \\ \overline{v}_t \\ \widetilde{\eta}_t \\ \widetilde{\xi}_t \end{pmatrix} = \begin{pmatrix} 0 & -\mathrm{i}(\mathbb{I}-\mathbb{P}_0) & 0 & 0 \\ \mathrm{i}(\mathbb{I}-\mathbb{P}_0) & 0 & 0 & 0 \\ 0 & 0 & 0 & \mathbb{P}_0 \\ 0 & 0 & -\mathbb{P}_0 & 0 \end{pmatrix} \begin{pmatrix} H_v \\ H_{\overline{v}} \\ H_{\widetilde{\eta}} \\ H_{\widetilde{\xi}} \end{pmatrix},$$

where $\mathbb{I}$ is the identity operator.

The next step introduces the modulational Ansatz

$$v = \varepsilon u(X,t)e^{\mathrm{i}k_0 x}, \qquad \overline{v} = \varepsilon\overline{u}(X,t)e^{-\mathrm{i}k_0 x}, \tag{18}$$
$$\widetilde{\eta} = \varepsilon^2\widetilde{\eta}_1(X,t), \qquad \widetilde{\xi} = \varepsilon\widetilde{\xi}_1(X,t), \tag{19}$$

which implies that we look for solutions in the form of quasi-monochromatic waves with carrier wavenumber $k_0 > 0$ and with slowly varying amplitude depending on $X = \varepsilon x$. Wave steepness is measured by the small parameter $\varepsilon \sim k_0 a_0 \ll 1$ where a_0 is a characteristic wave amplitude. The corresponding equations of motion read

$$\begin{pmatrix} u_t \\ \overline{u}_t \\ \widetilde{\eta}_{1t} \\ \widetilde{\xi}_{1t} \end{pmatrix} = \begin{pmatrix} 0 & -\mathrm{i}\varepsilon^{-1} & 0 & 0 \\ \mathrm{i}\varepsilon^{-1} & 0 & 0 & 0 \\ 0 & 0 & 0 & \varepsilon^{-2} \\ 0 & 0 & -\varepsilon^{-2} & 0 \end{pmatrix} \begin{pmatrix} H_u \\ H_{\overline{u}} \\ H_{\widetilde{\eta}_1} \\ H_{\widetilde{\xi}_1} \end{pmatrix}. \tag{20}$$

3.2. Expansion of the Hamiltonian

The modulational Ansatz (18)–(19) also introduces the small parameter ε in the expression of the Hamiltonian (13) which can then be expanded in powers of ε. Up to order $O(\varepsilon^3)$, we find

$$\begin{aligned} H = \frac{\varepsilon}{2}\int_{-\infty}^{\infty} \Big[& \overline{u}\Big(\omega(k_0) + \varepsilon\omega_k(k_0)D_X + \frac{\varepsilon^2}{2}\omega_{kk}(k_0)D_X^2\Big)u + \text{c.c.} \\ & + \varepsilon^2\Big\{\frac{1}{2}G_0(k_0)\Big(G_0(k_0)G_0(2k_0) - k_0^2\Big) - \frac{5\mathcal{D}}{4\rho}k_0^6 a^{-4}(k_0)\Big\}|u|^4 \\ & + \varepsilon^2\Big(2\mathrm{i}k_0 D_X\widetilde{\xi}_1 + \Big\{k_0^2 - G_0^2(k_0)\Big\}a^2(k_0)\widetilde{\eta}_1\Big)|u|^2 \\ & + \varepsilon^2\Big(h\widetilde{\xi}_1 D_X^2\widetilde{\xi}_1 + g\widetilde{\eta}_1^2\Big)\Big]dX + O(\varepsilon^4), \end{aligned} \tag{21}$$

where c.c. stands for the complex conjugate of all the preceding terms on the right-hand side of the equation, and the coefficient

$$\omega(k) = \sqrt{G_0(g + \mathcal{D}k^4/\rho)},$$

denotes the linear dispersion relation in terms of the angular frequency. For convenience, we also use the notation $k = l$ for the wavenumber in the x-direction. The scale separation lemma of[4] is applied to homogenize the fast oscillations in x and retain the four-wave resonant terms. Note the mean-flow contributions to this order of approximation in (21).

The Hamiltonian (21) can be further reduced by subtracting a multiple of the wave action

$$M = \varepsilon \int_{-\infty}^{\infty} |u|^2 dX, \tag{22}$$

together with a multiple of the impulse

$$I = \varepsilon \int_{-\infty}^{\infty} \Big[k_0|u|^2 + \frac{\varepsilon}{2}\Big(\overline{u}D_X u + u\overline{D_X u}\Big) + \mathrm{i}\varepsilon^2\widetilde{\eta}_1 D_X\widetilde{\xi}_1\Big]dX + O(\varepsilon^4),$$

so that it simplifies to

$$\begin{aligned}\widetilde{H} &= H - \omega_k(k_0)I - \Big(\omega(k_0) - k_0\omega_k(k_0)\Big)M,\\ &= \frac{\varepsilon^3}{2}\int_{-\infty}^{\infty}\Big[\omega_{kk}(k_0)\overline{u}D_X^2 u + \Big\{\frac{1}{2}G_0(k_0)\Big(G_0(k_0)G_0(2k_0) - k_0^2\Big) - \frac{5\mathcal{D}}{4\rho}k_0^6 a^{-4}(k_0)\Big\}|u|^4\\ &\quad + \Big\{2\mathrm{i}k_0 D_X\widetilde{\xi}_1 + \Big(k_0^2 - G_0^2(k_0)\Big)a^2(k_0)\widetilde{\eta}_1\Big\}|u|^2\\ &\quad + h\widetilde{\xi}_1 D_X^2\widetilde{\xi}_1 + g\widetilde{\eta}_1^2 - 2\mathrm{i}\omega_k(k_0)\widetilde{\eta}_1 D_X\widetilde{\xi}_1\Big]dX + O(\varepsilon^4).\end{aligned} \tag{23}$$

The subtraction of M from H reflects the fact that our approximation to the problem is phase invariant, while the subtraction of I is equivalent to changing the coordinate system into a reference frame moving with the group velocity $\omega_k(k_0)$.

3.3. NLS equation

Accordingly, Eqs. (20) take the reduced form

$$\begin{aligned}\mathrm{i}u_\tau &= \frac{1}{2}\omega_{kk}(k_0)D_X^2 u + \Big[\frac{1}{2}G_0(k_0)\Big(G_0(k_0)G_0(2k_0) - k_0^2\Big) - \frac{5\mathcal{D}}{4\rho}k_0^6 a^{-4}(k_0)\Big]u|u|^2\\ &\quad + \Big[\mathrm{i}k_0 D_X\widetilde{\xi}_1 + \frac{1}{2}\Big(k_0^2 - G_0^2(k_0)\Big)a^2(k_0)\widetilde{\eta}_1\Big]u,\end{aligned} \tag{24}$$

$$\varepsilon\widetilde{\eta}_{1\tau} = -\mathrm{i}k_0 D_X|u|^2 + hD_X^2\widetilde{\xi}_1 + \mathrm{i}\omega_k(k_0)D_X\widetilde{\eta}_1, \tag{25}$$

$$\varepsilon\widetilde{\xi}_{1\tau} = -\frac{1}{2}\Big(k_0^2 - G_0^2(k_0)\Big)a^2(k_0)|u|^2 + \mathrm{i}\omega_k(k_0)D_X\widetilde{\xi}_1 - g\widetilde{\eta}_1, \tag{26}$$

where $\tau = \varepsilon^2 t$. To leading order in ε, the right-hand side of (25) equals zero. Then integrating this equation with respect to X assuming vanishing conditions at infinity (as is the case for solitary waves), we obtain

$$\mathrm{i}k_0|u|^2 - hD_X\widetilde{\xi}_1 - \mathrm{i}\omega_k(k_0)\widetilde{\eta}_1 = 0. \tag{27}$$

Similarly, from (26), we have

$$\frac{1}{2}\Big(k_0^2 - G_0^2(k_0)\Big)a^2(k_0)|u|^2 - \mathrm{i}\omega_k(k_0)D_X\widetilde{\xi}_1 + g\widetilde{\eta}_1 = 0. \tag{28}$$

Solving (27)–(28) for $D_X\widetilde{\xi}_1$ and $\widetilde{\eta}_1$ leads to

$$D_X\widetilde{\xi}_1 = -\frac{\mathrm{i}}{h}\Big[\frac{\omega_k^2(k_0)}{h} - g\Big]^{-1}\Big[gk_0 + \frac{1}{2}\omega_k(k_0)\Big(k_0^2 - G_0^2(k_0)\Big)a^2(k_0)\Big]|u|^2, \tag{29}$$

and

$$\widetilde{\eta}_1 = \Big[\frac{\omega_k^2(k_0)}{h} - g\Big]^{-1}\Big[\frac{1}{2}\Big(k_0^2 - G_0^2(k_0)\Big)a^2(k_0) + \frac{k_0\omega_k(k_0)}{h}\Big]|u|^2. \tag{30}$$

Finally, substituting (29)–(30) into (24) results in the NLS equation

$$\mathrm{i}u_\tau + \lambda u_{XX} + \mu|u|^2u = 0, \tag{31}$$

whose coefficients are given by

$$\lambda = \frac{1}{2}\omega_{kk}(k_0), \tag{32}$$

$$\begin{aligned}\mu = {} & \frac{1}{2}G_0(k_0)\Big(k_0^2 - G_0(k_0)G_0(2k_0)\Big) + \frac{5\mathcal{D}}{4\rho}k_0^6a^{-4}(k_0) \\ & + \frac{k_0}{h}\Big[g - \frac{\omega_k^2(k_0)}{h}\Big]^{-1}\Big[gk_0 + \frac{1}{2}\omega_k(k_0)\Big(k_0^2 - G_0^2(k_0)\Big)a^2(k_0)\Big] \\ & + \frac{1}{2}\Big(k_0^2 - G_0^2(k_0)\Big)a^2(k_0)\Big[g - \frac{\omega_k^2(k_0)}{h}\Big]^{-1}\Big[\frac{1}{2}\Big(k_0^2 - G_0^2(k_0)\Big)a^2(k_0) + \frac{k_0\omega_k(k_0)}{h}\Big],\end{aligned} \tag{33}$$

and the corresponding Hamiltonian is

$$H = \int_{-\infty}^{\infty}\Big(\lambda|u_X|^2 - \frac{\mu}{2}|u|^4\Big)dX. \tag{34}$$

According to (17), the ice-sheet deflection can be expressed in terms of u as

$$\eta(X,\tau) = \frac{\varepsilon}{\sqrt{2}}\left[\sqrt[4]{\frac{(k_0+\varepsilon D_X)\tanh(h(k_0+\varepsilon D_X))}{g+\mathcal{D}(k_0+\varepsilon D_X)^4/\rho}}\,u(X,\tau)e^{\mathrm{i}k_0X/\varepsilon} + \text{c.c.}\right] + \varepsilon^2\widetilde{\eta}_1, \tag{35}$$

where the mean component $\widetilde{\eta}_1$ is given by (30).

3.4. Envelope soliton solutions

Equation (31) is of focusing type, and thus admits solitary wave solutions travelling at the group velocity $\omega_k(k_0)$, if $\lambda\mu > 0$. For infinite depth, it was found in [12] that

$$\begin{aligned}\lambda &= \frac{5\mathcal{D}k_0^3}{\rho\sqrt{gk_0 + \mathcal{D}k_0^5/\rho}} - \frac{(g+5\mathcal{D}k_0^4/\rho)^2}{8(gk_0+\mathcal{D}k_0^5/\rho)^{3/2}}, \\ &= \frac{15(\mathcal{D}/\rho)^2}{8(gk_0+\mathcal{D}k_0^5/\rho)^{3/2}}\left[k_0^4 + \left(1+\frac{4}{\sqrt{15}}\right)3k_{\min}^4\right]\left[k_0^4 + \left(1-\frac{4}{\sqrt{15}}\right)3k_{\min}^4\right],\end{aligned}$$

$$\mu = \frac{5\mathcal{D}k_0^7}{4\rho(g+\mathcal{D}k_0^4/\rho)} - \frac{k_0^3}{2} = \frac{3\mathcal{D}k_0^3/\rho}{4\left(g+\mathcal{D}k_0^4/\rho\right)}\left(k_0^4 - 2k_{\min}^4\right),$$

which implies that $\lambda\mu < 0$, since $\lambda > 0$ and $\mu < 0$ if

$$k_0 = k_{\min} = \left(\frac{g\rho}{3\mathcal{D}}\right)^{1/4}.$$

Therefore, solitary waves are not predicted by (31) in that case.

However, in finite depth, λ is always positive for $k_0 = k_{\min}$, while the sign of μ depends on the depth h. There exists a critical depth h_c where $\mu = 0$, implying that higher-order terms need to be included in the equation. We will not consider this higher-order situation here. For $h > h_c$, the coefficient μ is negative and Eq. (31) is defocusing, which is

consistent with results found in the infinite-depth limit [19,12]. For $h < h_c$, the coefficient μ is positive and thus Eq. (31) admits solitary wave solutions.

In view of comparing with (steady) fully nonlinear solutions, as discussed in the next section, we consider the exact NLS soliton

$$u(X,\tau) = \sqrt{2}u_0 \mathrm{sech}\left(u_0\sqrt{\frac{\mu}{\lambda}}X\right)e^{i\mu u_0^2\tau}, \tag{36}$$

which corresponds to solitary waves whose crests are stationary relative to their envelopes [1].

We point out that the mean components (29) and (30), and hence the NLS equation (31) together with its solution (36), are well-defined provided the group velocity $\omega_k(k_0)$ does not equal the long-wave limit $c_0 = \sqrt{gh}$.

4. Numerical results

For numerical purposes, we non-dimensionalise (1)–(5) using the characteristic scales

$$\mathcal{L} = \left(\frac{\mathcal{D}}{\rho g}\right)^{1/4}, \qquad \mathcal{V} = \left(\frac{\mathcal{D}g^3}{\rho}\right)^{1/8},$$

as unit length and unit velocity, respectively, so that $g = 1$ and $\mathcal{D}/\rho = 1$ after non-dimensionalisation [25,2,19]. Since we are interested in solitary waves, the key parameters which are examined in the problem are the dimensionless wave speed c and the dimensionless water depth h. The dimensionless value of the critical depth in the NLS regime is $h_c = 8.773$, which is comparable to the value $h_c = 7.63$ found by Părău and Dias [22] in the Kirchhoff–Love case.

Fully nonlinear computations of stationary solitary waves in a reference frame moving at speed c are carried out using a boundary-integral method combined with Cauchy's integral formula, while simulations of time-evolving solitary waves are performed using a high-order spectral method based on the Hamiltonian equations (10)–(11). In the latter situation, unforced (i.e. freely propagating) solitary waves are generated by initially applying a localised pressure distribution of the form

$$P = P_0 e^{-(x-ct)^2/16}, \tag{37}$$

over a finite period of time (typically $0 \le t \le 125$), while forced solitary waves are produced by continuously applying (37) throughout the entire simulation. In either case, the pressure term (37) is added to the right-hand side of (11). These numerical methods are described in [11,29,12,13], and therefore the reader is referred to these articles for further details.

We present results for shallow and deep water, and only consider $c < c_{\min}$. Depression and elevation solitary waves were found in all cases, but as the elevation branch was found to be unstable and it has a more complicated behaviour (see [27]), we concentrate here on the depression waves.

In Fig. 1, we plot the amplitude of steady forced and unforced depression waves for $h = \infty$ and $h = 1$. A steady version of (37) was used in the forced case as in [12]. For infinite depth, $c_{\min} = 2/3^{3/8} \approx 1.325$ and, for $h = 1$, $c_{\min} = 0.987$. Some differences can be observed between these two cases. The branch of depression solitary waves starts at a finite amplitude in the infinite-depth case, while it starts from zero for $h = 1$. The branch of forced waves for $P_0 = 0.01$, which is continuous for $h = 1$, is split into two disconnected branches in infinite depth. One of these branches is a perturbation of the uniform flow and the other is a perturbation of the pure solitary wave. In the limit $c \to 0$, the deep-water branch tends to a self-intersecting profile with an amplitude of about 2.7, while the shallow-water branch does not overturn and its amplitude is bounded by the fluid depth (which is $h = 1$). Some typical profiles of forced and unforced solutions are shown in Fig. 2.

In Fig. 3, we plot the energy H in the two cases $h = \infty$ and $h = 1$ for unforced depression solitary waves ($P_0 = 0$). It can be observed that, in deep water, there is an energy minimum at about $c \approx 1.31$ while, in shallow water, the branch monotonically decays for $c < c_{\min}$ in the neighbourhood of $c_{\min}$. Other energy extrema were also found for c close to 0 (see e.g. Fig. 5(b) in [12] for infinite depth).

A comparison between a fully nonlinear steady wave computed with the boundary-integral method and an NLS soliton solution given by (35)–(36) is presented in Fig. 4 for $h = 1$ and $c = 0.985$. As in [13], we set $\varepsilon = 1$ and vary u_0 in (35)–(36) to fit the fully nonlinear solution as closely as possible, which implies that the NLS wave steepness is

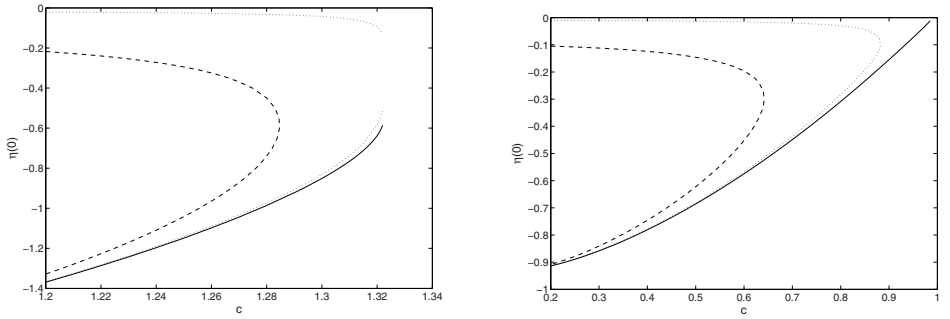

Fig. 1. Amplitudes of steady depression solitary waves for $h = \infty$ (left) and $h = 1$ (right). The solid line represents pure (unforced) solitary waves with $P_0 = 0$, the dashed line represents forced solitary waves with $P_0 = 0.1$ and the dotted line represents forced solitary waves with $P_0 = 0.01$.

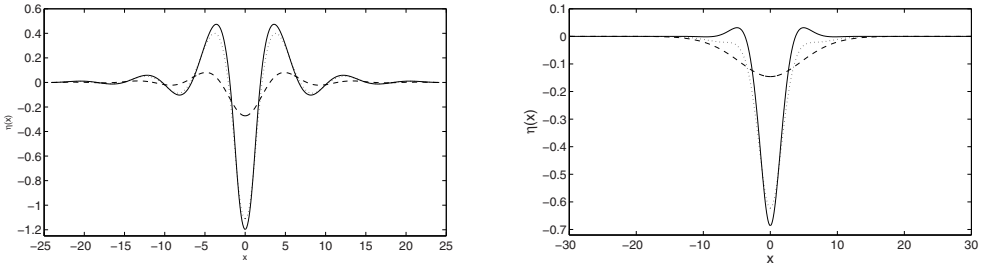

Fig. 2. Examples of steady forced and unforced depression solitary waves for $h = \infty$, $c = 1.24$ (left) and $h = 1$, $c = 0.5$ (right). The solid line represents pure (unforced) solitary waves with $P_0 = 0$, the dashed line represents forced solitary waves with $P_0 = 0.1$ and the dotted line represents forced solitary waves with $P_0 = 0.01$.

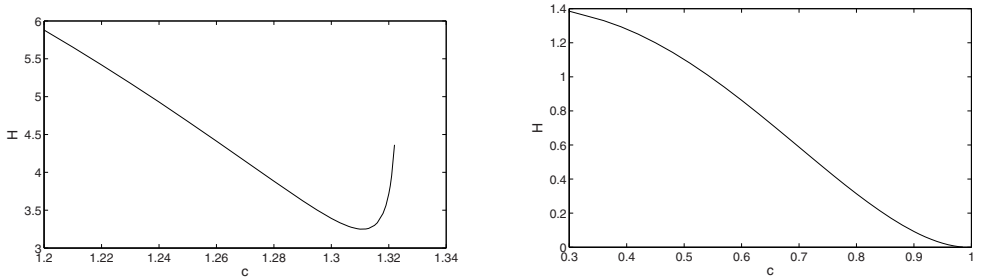

Fig. 3. Energy of steady depression solitary waves for $h = \infty$ (left) and $h = 1$ (right).

measured by u_0. A good agreement is found, especially regarding the relative amplitude of the central trough and the wavelength.

In Fig. 5, we plot the amplitude of steady depression solitary waves for a fixed $c = 0.9$ but varying h. It is observed that the amplitude increases with h, which may be explained by the fact that $c_{\min}$ increases with h and $c = 0.9$ is far away from this critical speed.

Turning our attention to time-dependent simulations, Fig. 6 shows snapshots of a large-amplitude freely propagating solitary wave of depression, induced by a pressure of amplitude $P_0 = 0.1$ in the shallow-water case $h = 1.5$. This solution seems to be stable, travelling with a well-defined localised shape at near-constant speed among background

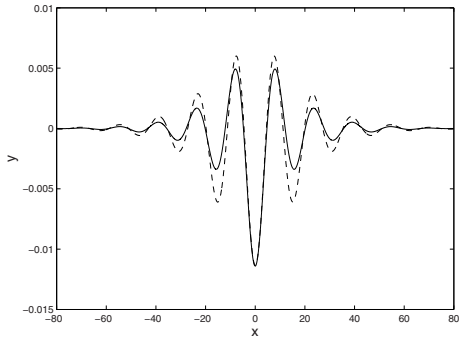

Fig. 4. Comparison of steady wave profiles obtained from the boundary-integral method (solid line) and from the NLS soliton as given by (35)–(36) (dashed line) for $h = 1$ and $c = 0.985$.

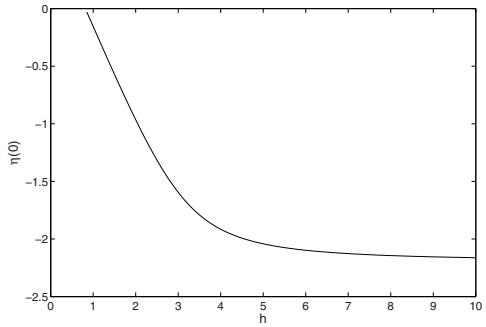

Fig. 5. Amplitude of steady depression solitary waves for $c = 0.9$ as a function of h.

radiation (which was also excited by the initial forcing). Note that the pressure speed was set to $c = 0.9$ but, after the forcing is removed at $t = 125$, the speed of the resulting solitary wave is found to be lower, that is $c \approx 0.658$. The solitary wave profile in Fig. 6 compares well with the steady one computed by the boundary-integral method [13], and similar solutions were obtained for other values of h including the infinite-depth limit [12].

For this case, the conservation of invariants of motion (i.e. energy H, impulse I and volume V) after $t = 125$ is illustrated in Fig. 7. We see that all three quantities are very well conserved in time, with V being essentially zero as for gravity-capillary water waves [17].

Finally, Fig. 8 shows snapshots of a continuously forced solution by a pressure of amplitude $P_0 = 0.1$ and speed $c = 0.8$, for $h = 1$. This solution evolves into an elevation front (or bore) moving ahead of the forcing disturbance at speed ~ 1.089, followed by a train of depression solitary waves trailing behind the pressure distribution. These trailing solitary waves have similar characteristics and, as time progresses, an increasingly larger number of them are produced by the forcing.

5. Conclusions

The Hamiltonian formulation for three-dimensional fully nonlinear flexural-gravity waves propagating at the surface of an ideal fluid covered by an ice sheet was presented. The ice cover is modelled as a thin elastic sheet, based on the special Cosserat theory for hyperelastic shells as proposed by Plotnikov and Toland [21]. A cubic NLS equation for two-dimensional weakly nonlinear waves travelling with speeds near the minimum phase velocity $c_{\min}$ was

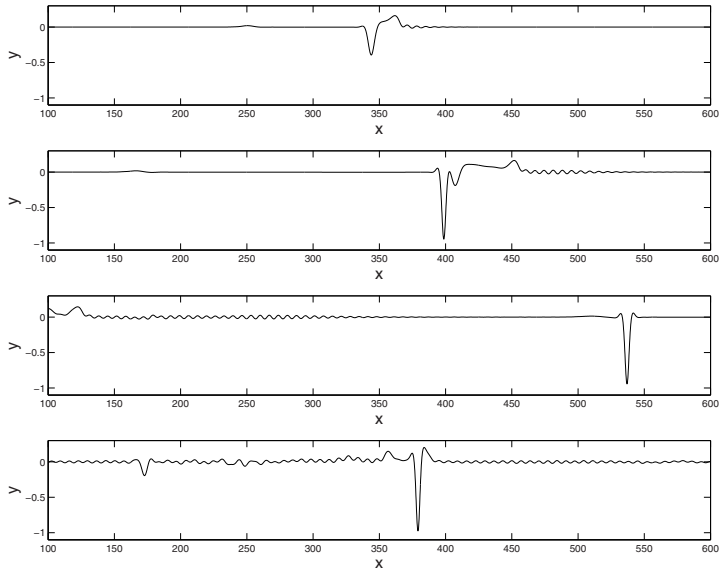

Fig. 6. Snapshots of an unforced solution at $t = 50, 120, 330, 1000$ (from top to bottom) for $P_0 = 0.1$, $c = 0.658$ and $h = 1.5$. The solid line represents the ice-sheet deflection $\eta(x, t)$. The pressure is removed at $t = 125$.

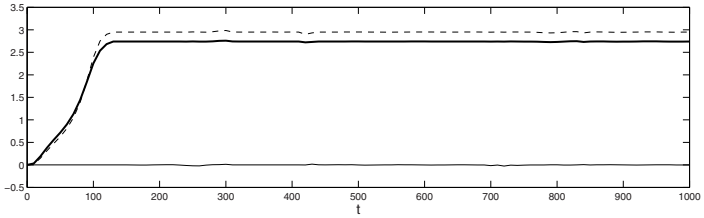

Fig. 7. Time evolution of energy H (thick solid line), impulse I (dashed line) and volume V (thin solid line) for $P_0 = 0.1$, $c = 0.658$ and $h = 1.5$. The pressure is removed at $t = 125$.

derived. There is a transition between shallow and deep water, where the nonlinear coefficient of this NLS equation changes sign. Fully nonlinear forced and unforced solitary waves were also computed in this two-dimensional regime. Differences between shallow- and deep-water cases were highlighted.

Acknowledgements

P. Guyenne is partially supported by the Simons Foundation under grant 246170. E.I. Părău is supported by the EPSRC under grant EP/J019305/1.

References

1. Akylas, T., 1993. Envelope solitons with stationary crests. Phys. Fluids 5, 789–791.
2. Bonnefoy, F., Meylan, M., Ferrant, P., 2009. Nonlinear higher-order spectral solution for a two-dimensional moving load on ice. J. Fluid Mech. 621, 215–242.

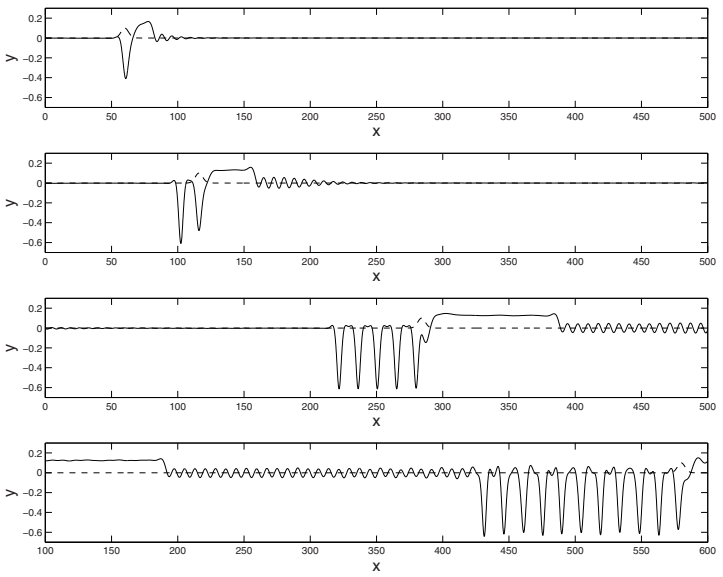

Fig. 8. Snapshots of a forced solution at $t = 50, 120, 330, 700$ (from top to bottom) for $P_0 = 0.1$, $c = 0.8$ and $h = 1$. The solid line represents the ice-sheet deflection $\eta(x, t)$ while the dashed line represents the pressure distribution (37).

3. Craig, W., Guyenne, P., Kalisch, H., 2005. Hamiltonian long wave expansions for free surfaces and interfaces. Commun. Pure Appl. Math. 58, 1587–1641.
4. Craig, W., Guyenne, P., Nicholls, D., Sulem, C., 2005. Hamiltonian long-wave expansions for water waves over a rough bottom. Proc. R. Soc. A 461, 839–873.
5. Craig, W., Guyenne, P., Sulem, C., 2010. A Hamiltonian approach to nonlinear modulation of surface water waves. Wave Motion 47, 552–563.
6. Craig, W., Guyenne, P., Sulem, C., 2012. Hamiltonian higher-order nonlinear Schrödinger equations for broader-banded waves on deep water. Eur. J. Mech. B/Fluids 32, 22–31.
7. Craig, W., Schanz, U., Sulem, C., 1997. The modulational regime of three-dimensional water waves and the Davey–Stewartson system. Ann. Inst. H. Poincaré (C) Nonlin. Anal. 14, 615–667.
8. Craig, W., Sulem, C., 1993. Numerical simulation of gravity waves. J. Comput. Phys. 108, 73–83.
9. Forbes, L., 1986. Surface-waves of large amplitude beneath an elastic sheet. Part 1. High-order solutions. J. Fluid Mech. 169, 409–428.
10. Forbes, L., 1988. Surface-waves of large amplitude beneath an elastic sheet. Part 2. Galerkin solution. J. Fluid Mech. 188, 491–508.
11. Guyenne, P., Nicholls, D., 2007. A high-order spectral method for nonlinear water waves over moving bottom topography. SIAM J. Sci. Comput. 30, 81–101.
12. Guyenne, P., Părău, E., 2012. Computations of fully nonlinear hydroelastic solitary waves on deep water. J. Fluid Mech. 713, 307–329.
13. Guyenne, P., Părău, E., 2013. Finite-depth effects on solitary waves in a floating ice sheet. J. Fluid Struct. submitted, 1–30.
14. Haragus-Courcelle, M., Ilichev, A., 1998. Three-dimensional solitary waves in the presence of additional surface effects. Eur. J. Mech. B/Fluids 17, 739–768.
15. Hegarty, G., Squire, V., 2008. A boundary-integral method for the interaction of large-amplitude ocean waves with a compliant floating raft such as a sea-ice floe. J. Eng. Math. 62, 355–372.
16. Korobkin, A., Părău, E., Vanden-Broeck, J.-M., 2011. The mathematical challenges and modelling of hydroelasticity. Phil. Trans. R. Soc. Lond. A 369, 2803–2812.
17. Longuet-Higgins, M., 1989. Capillary-gravity waves of solitary type on deep water. J. Fluid Mech. 200, 451–470.
18. Marko, J., 2003. Observations and analyses of an intense waves-in-ice event in the Sea of Okhotsk. J. Geophys. Res. 108, 3296.
19. Milewski, P., Vanden-Broeck, J.-M., Wang, Z., 2011. Hydroelastic solitary waves in deep water. J. Fluid Mech. 679, 628–640.
20. Milewski, P., Wang, Z., 2013. Three dimensional flexural-gravity waves. Stud. Appl. Maths 131, 135–148.
21. Plotnikov, P. I., Toland, J. F., 2011. Modelling nonlinear hydroelastic waves. Phil. Trans. Roy. Soc. Lond. A 369, 2942–2956.
22. Părău, E., Dias, F., 2002. Nonlinear effects in the response of a floating ice plate to a moving load. J. Fluid Mech. 460, 281–305.
23. Părău, E. I., Vanden-Broeck, J.-M., 2011. Three-dimensional waves beneath an ice sheet due to a steadily moving pressure. Phil. Trans. Roy. Soc. Lond. A 369, 2973–2988.
24. Squire, V., Hosking, R., Kerr, A., Langhorne, P., 1996. Moving loads on ice plates. Kluwer.
25. Takizawa, T., 1985. Deflection of a floating sea ice sheet induced by a moving load. Cold Regions Sci. Tech. 11, 171–180.
26. Vanden-Broeck, J.-M., Părău, E., 2011. Two-dimensional generalised solitary waves and periodic waves under an ice sheet. Phil. Trans. Roy. Soc. Lond. A 369, 2957–2972.

27. Wang, Z., Vanden-Broeck, J.-M., Milewski, P., 2013. Two-dimensional flexural-gravity waves of finite amplitude in deep water. IMA J. Appl. Maths. 78, 750–761.
28. Xia, X., Shen, H., 2002. Nonlinear interaction of ice cover with shallow water waves in channels. J. Fluid Mech. 467, 259–268.
29. Xu, L., Guyenne, P., 2009. Numerical simulation of three-dimensional nonlinear water waves. J. Comput. Phys. 228, 8446–8466.
30. Zakharov, V. E., 1968. Stability of periodic waves of finite amplitude on the surface of a deep fluid. J. Appl. Mech. Tech. Phys. 9, 190–194.